

Negative magnetoresistance in the antiferromagneticsemimetal $V_{1/3}TaS_2$

Zi Wang(王子), Xin Peng(彭馨), Shengnan Zhang(张胜男), Yahui Su(苏亚慧), Shaodong Lai(赖少东), Xuan Zhou(周旋), Chunxiang Wu(吴春翔), Tingyu Zhou(周霆宇), Hangdong Wang(王杭栋), Jinhu Yang(杨金虎), Bin Chen(陈斌), Huifei Zhai(翟会飞), Quansheng Wu(吴泉生), Jianhua Du(杜建华), Zhiwei Jiao(焦志伟), and Minghu Fang(方明虎)

Citation: Chin. Phys. B, 2024, 33 (**3**): 037301. DOI: 10.1088/1674-1056/ad18aa
Journal homepage: http://cpb.iphy.ac.cn; http://iopscience.iop.org/cpb

What follows is a list of articles you may be interested in

Nonlinear current response and electric quantum oscillations in the Dirac semimetal Cd_3As_2

Hao-Nan Cui(崔浩楠), Ze-Nan Wu(吴泽南), Jian-Kun Wang(王建坤), Guang-Yu Zhu(祝光宇), Jia-Jie Yang(杨佳洁), Wen-Zhuang Zheng(郑文壮), Zhi-Min Liao(廖志敏), Shuo Wang(王硕), Ben-Chuan Lin(林本川), and Dapeng Yu(俞大鹏)

Chin. Phys. B, 2023, 32 (**8**): 087306. DOI: 10.1088/1674-1056/acd9c5

Electric modulation of anisotropic magnetoresistance in Pt/HfO_{2-x}/NiO_y/Ni heterojunctions

Xiaoyu Ye(叶晓羽), Xiaojian Zhu(朱小健), Huali Yang(杨华礼), Jipeng Duan(段吉鹏), Cui Sun(孙翠), and Run-Wei Li(李润伟)

Chin. Phys. B, 2023, 32 (**8**): 087305. DOI: 10.1088/1674-1056/acd2b6

Negative magnetoresistance in Dirac semimetal Cd_3As_2 with in-plane magnetic field perpendicular to current

Hao-Nan Cui(崔浩楠), Guang-Yu Zhu(祝光宇), Jian-Kun Wang(王建坤), Jia-Jie Yang(杨佳洁), Wen-Zhuang Zheng(郑文壮), Ben-Chuan Lin(林本川), Zhi-Min Liao(廖志敏), Shuo Wang(王硕), and Da-Peng Yu(俞大鹏)

Chin. Phys. B, 2023, 32 (**7**): 077305. DOI: 10.1088/1674-1056/accd50

Analytical formula describing the non-saturating linear magnetoresistance in inhomogeneous conductors

Shan-Shan Chen(陈珊珊), Yang Yang(杨阳), and Fan Yang(杨帆)

Chin. Phys. B, 2022, 31 (**8**): 087303. DOI: 10.1088/1674-1056/ac6582

Bias-induced reconstruction of hybrid interface states in magnetic molecular junctions

Ling-Mei Zhang(张令梅), Yuan-Yuan Miao(苗圆圆), Zhi-Peng Cao(曹智鹏), Shuai Qiu(邱帅), Guang-Ping Zhang(张广平), Jun-Feng Ren(任俊峰), Chuan-Kui Wang(王传奎), and Gui-Chao Hu(胡贵超)

Chin. Phys. B, 2022, 31 (**5**): 057303. DOI: 10.1088/1674-1056/ac3caf

---

Negative magnetoresistance in the antiferromagnetic semimetal $V_{1/3}TaS_2$

Zi Wang(王子)[1,†], Xin Peng(彭馨)[1,†], Shengnan Zhang(张胜男)[2], Yahui Su(苏亚慧)[1], Shaodong Lai(赖少东)[1], Xuan Zhou(周旋)[1], Chunxiang Wu(吴春翔)[3], Tingyu Zhou(周霆宇)[3], Hangdong Wang(王杭栋)[4], Jinhu Yang(杨金虎)[4], Bin Chen(陈斌)[4], Huifei Zhai(翟会飞)[1], Quansheng Wu(吴泉生)[2,5], Jianhua Du(杜建华)[1,‡], Zhiwei Jiao(焦志伟)[1,§], and Minghu Fang(方明虎)[3,6,¶]

[1] *Department of Physics, China Jiliang University, Hangzhou* 310018, *China*
[2] *Beijing National Laboratory for Condensed Matter Physics and Institute of Physics, Chinese Academy of Sciences, Beijing* 100190, *China*
[3] *Department of Physics, Zhejiang University, Hangzhou* 310027, *China*
[4] *Department of Physics, Hangzhou Normal University, Hangzhou* 310036, *China*
[5] *University of Chinese Academy of Sciences, Beijing* 100049, *China*
[6] *Collaborative Innovation Center of Advanced Microstructure, Nanjing* 210093, *China*

(Received 2 November 2023; revised manuscript received 22 December 2023; accepted manuscript online 26 December 2023)

Intercalated transition metal dichalcogenides (TMDCs) attract much attention due to their rich properties and potential applications. In this article, we grew successfully high-quality $V_{1/3}TaS_2$ crystals by a vapor transport method. We measured the magnetization, longitudinal resistivity $\rho_{xx}(T,H)$, Hall resistivity $\rho_{xy}(T,H)$, as well as performed calculations of the electronic band structure. It was found that $V_{1/3}TaS_2$ is an A-type antiferromagnet with the Neel temperature $T_N = 6.20$ K, and exhibits a negative magnetoresistance (MR) near T_N. Both band structure calculations and Hall resistivity measurements demonstrated it is a magnetic semimetal.

Keywords: magnetoresistance, antiferromagnetic semimetal, band structure

PACS: 73.43.Qt, 71.20.–b, 75.50.Ee, 71.55.Ak **DOI:** 10.1088/1674-1056/ad18aa

1. Introduction

The recent discoveries of both long-range magnetic ordering in the atomically thin layers of $Cr_2Ge_2Te_6$,[1] CrI_3,[2] and Fe_3GeTe_2,[3,4] and the chiral solitons in $Cr_{1/3}NbS_2$[5,6] and $Fe_{1/4}TaS_2$[7] rekindle interest in the intercalated transition metal dichalcogenides (TMDCs). TMDCs are a class of layered materials, whose structure can be classified into 1H (triangular prismatic), 1T (octahedral), 2H (hexagonal), 3R (rhombic), and so on, depending on the local coordination of atoms around the central transition metal atoms. The intercalation (or doping) of atoms (or molecules) can modulate the physical properties of materials,[8–10] such as, the Cu intercalation in $TiSe_2$, leads to superconductivity,[11] the Fe, Cr intercalations of TaS_2 or NbS_2 result in long-range magnetic order.[12,13] More interestingly, the Cr intercalation in NbS_2 leads to the chiral soliton lattice formation due to the antisymmetric Dzyaloshinskii–Moriya (DM) interactions. TMDCs become a material platform for exploring various exotic physical properties.

In these TMDCs, the M_xTS_2 (M = 3d transition metal, T = Ta, Nb) family[14] with $x = 1/3$ exhibit unique properties, due to the inserted ionic arranging in a stacked $\sqrt{3} \times \sqrt{3}$ superlattice, reducing the crystal symmetry.[15] For example, a chiral helical magnetic order was observed in $Cr_{1/3}NbS_2$,[5] a large anomalous Hall effect occurs in $Co_{1/3}NbS_2$.[16] In this article, on the basis of growing successfully high-quality $V_{1/3}TaS_2$ crystals, we carried out the magnetization, longitudinal, and Hall resistivity measurements, combined with the electronic band structure calculations. It was found that $V_{1/3}TaS_2$ is an A-type antiferromagnet (AFM) with the Neel temperature $T_N = 6.20$ K, a single magnetic transition, which is different from the multi-transitions due to the existence of impurities or disorder, reported in the previous literature.[17] We also observed the negative magnetoresistance (MR) occurring near T_N, resulting from the suppression of spin-scattering by an external magnetic field. It is interesting that both band structure calculations and Hall resistivity measurements demonstrate it is a magnetic semimetal.

2. Methods

$V_{1/3}TaS_2$ single crystals were grown by a chemical vapor transport method with two steps. First, polycrystalline samples were prepared by using a stoichiometric of V (99.9%), Ta (99.9%), and S (99.99%) powders, whose mixtures were

[†]These authors contributed equally to this work.
[‡]Corresponding author. E-mail: jhdu@cjlu.edu.cn
[§]Corresponding author. E-mail: jiaozw@cjlu.edu.cn
[¶]Corresponding author. E-mail: mhfang@zju.edu.cn

© 2024 Chinese Physical Society and IOP Publishing Ltd

sealed in an evacuated silica tube and heated at 1073 K for a week. Second, the evacuated silica tube containing the polycrystalline powders with iodine as transport agent (10 mg/cm^3) was placed in a tube furnace, and heated for 7 days with a temperature gradient from 1223 K to 1123 K. The hexagonal crystals were obtained at the cold end, whose typical dimensions are 2 mm × 1 mm × 0.2 mm (see the inset of Fig. 1(d)). The composition of crystals was determined by the energy-dispersive x-ray (EDX) technique, as shown in Fig. 1(c), to be of V:Ta:S = 1:3:6. The crystal structure was checked by both polycrystalline (not shown) and single crystal x-ray diffraction (XRD), as shown in Fig. 1(d). The (00l) peaks with a small width at half maximum were observed, indicating that the obtained crystals have high quality. The length of the c-axis was estimated to be 11.19 Å, which is similar to that reported previously.[17]

The longitudinal and Hall resistivity and magnetization measurements were carried out on the quantum design physical property measurement system (PPMS-9T) and magnetic property measurement system (MPMS-7T), respectively. To calculate the electronic band structure, and Fermi surface of bulk $V_{1/3}TaS_2$, the Vienna *ab initio* simulation package (VASP)[18,19] with the generalized gradient approximation of Perdew, Burke, and Ernzerhof for the exchange–correlation potential[20] was employed to perform the first-principles calculations based on the density functional theory (DFT). The projector-augmented wave (PAW) potentials were adopted for the inner electrons[21] and the cores of S:(Ne, $3s^2 3p^4$), Ta:(Xe, $6s^1 5d^4$), and V:(Ar, $4s^1 3d^4$) have been used in the calculations. The kinetic energy cut off was chosen as 360 eV for the wave function, and the Γ-centered mesh $6 \times 6 \times 4$ was used to calculate the electronic structures. The tolerance of energy convergence was chosen to be 10^{-6} eV.

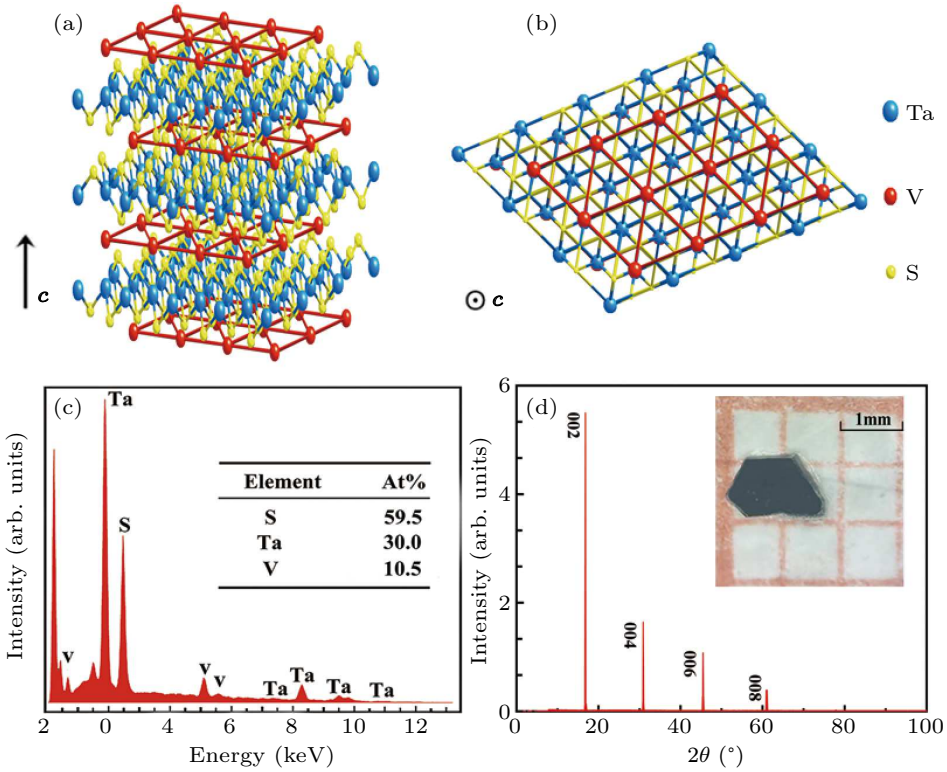


Fig. 1. (a) Side view of crystal structure with V atoms intercalated between the TaS_2 layers. (b) Top view of crystal structure along the c-axis. (c) Energy dispersive x-ray spectrometer (EDXS) for the $V_{1/3}TaS_2$ crystal. (d) Single crystal XRD pattern. Inset: the photograph of a crystal.

3. Results and discussion

Figures 1(a) and 1(b) show the crystal structure of $V_{1/3}TaS_2$, a hexagonal non-centrosymmetric structure, where the V^{3+} ions occupy the octahedral position and intercalate between the triangular prismatic layers of the parent 2H-TaS_2, forming a superlattice of $\sqrt{3} \times \sqrt{3}$ structure with lower symmetry. The host TaS_2 layer provides conduction electrons, while the orbital moment of V^{3+} is usually quenched due to the octahedral crystal fields of neighboring S^{2-}, and the localized moment of V^{3+} mainly originates from the spins of the unpaired electrons.

In order to understand well the physical properties of $V_{1/3}TaS_2$ compound, we calculate its electronic band structure. Figure 2(a) shows the band structure of the A-type AFM phase with considering spin–orbit coupling (SOC). It is clear that the Fermi energy level (E_F) locates in the conduction band, indicating a metallic behavior, there are three hole pockets (the left, near the Γ and A points) and one electron pocket (near the K point), and the results reveal that it is antiferromagnetic out-of-plane and ferromagnetic in-plane. These results

demonstrate that $V_{1/3}TaS_2$ is a magnetic semimetal.

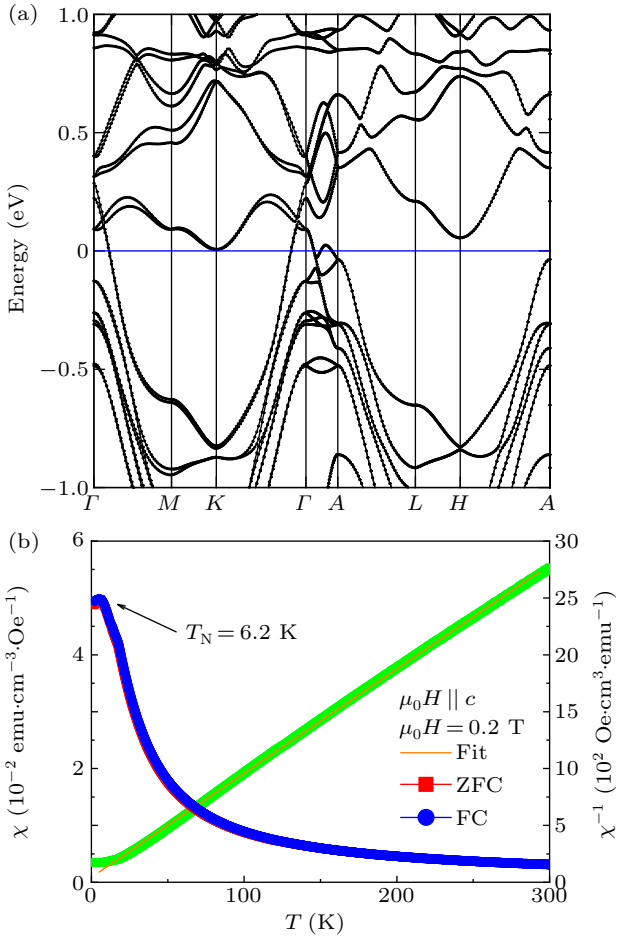


Fig. 2. (a) The calculated band structure with SOC. (b) Temperature dependence of magnetic susceptibility, $\chi = M/H$, measured at $H = 2000$ Oe applied along the c-axis with both ZFC and FC processes. The right axis is for $\chi^{-1}(T)$.

Next, we discuss the results of magnetization measurements. Figure 2(b) shows the temperature dependence of magnetic susceptibility, $\chi = M/H$, measured at a magnetic field of $H = 2000$ Oe applied along the c-axis with zero-field-cooling (ZFC) and field-cooling (FC) processes. Although the $\chi(T)$ curves measured with ZFC and FC processes seem to overlap with each other, small differences at low temperatures can be recognized in the magnified $\chi(T)$ curves (not shown). With decreasing temperature, the susceptibility increases continuously for both processes. A sharp peak occurs at $T_N = 6.2$ K in the $\chi(T)$ curves, corresponding to an antiferromagnetic transition. The susceptibility above T_N follows the Curie–Weiss law

$$\chi = \frac{C}{T - \theta}, \tag{1}$$

where C is the molar Curie constant and θ is the Weiss temperature. Figure 2(b) (the right axis) shows the temperature dependence of inverse susceptibility, $\chi^{-1}(T)$, exhibiting a linear temperature dependence. We obtained that $C \approx 0.11$ cm^3·K·mol^{-1}, corresponding to the effective moment $\mu_{\text{eff}} \approx 2.7\ \mu_B/V^{3+}$, and $\theta \approx 3.8$ K, close to T_N value, by fitting the $\chi^{-1}(T)$ data between 10 K–300 K. Different from the observations that two magnetic transitions emerge in the polycrystalline or as-grown $V_{1/3}TaS_2$ single crystals, only one transition was observed in our crystals, implying our crystal has high quality (no impurities or disorders). Early, $V_{1/3}TaS_2$ was identified as a ferromagnet by Parkin *et al.*,[22] similar to that suggested for other intercalated TMDCs, such as, $Cr_{1/3}TaS_2$, a soliton candidate;[13] $Mn_{1/3}NbS_2$, a ferromagnet with a long period spin modulation.[23] Recently, based on their magnetization and neutron diffraction results on a single crystal of $V_{1/3}TaS_2$, Lu *et al.*[17] suggested that $V_{1/3}TaS_2$ is an A-type antiferromagnet, composed of a staggered stacking of ferromagnetic planes, with a small out-of-plane canted (2°) of XY spins and the Neel temperature $T_N = 32$ K. Although the T_N value here is different from that reported by Lu *et al.*,[17] we believe that the magnetic structure at low temperatures is the same as that determined by their neutron diffraction and the exchange interaction analysis, i.e., an antiferromagnetic stacking of ferromagnetic planes with a small canting of V^{3+} spins (A-type AFM).

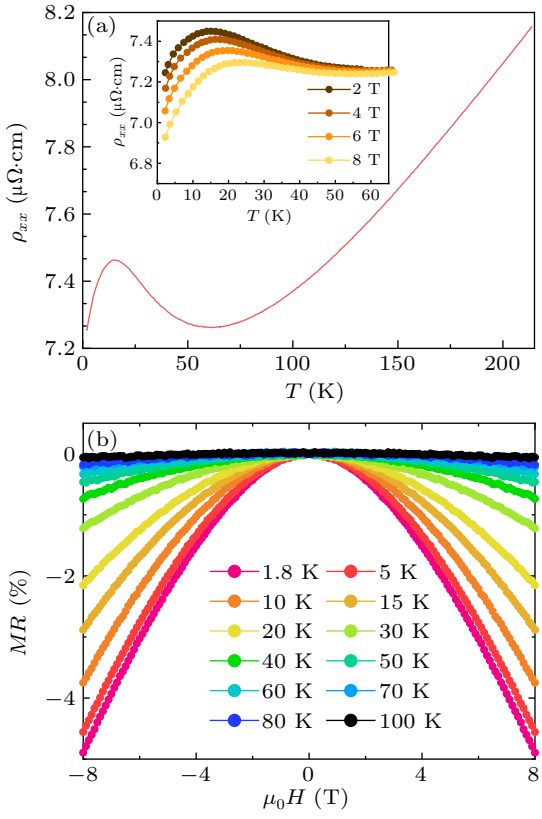


Fig. 3. (a) Temperature dependence of longitudinal resistivity ρ_{xx} measured at zero field, the inset shows resistivity measured at various magnetic fields. (b) Field dependence of MR at various temperatures with a magnetic field applied along the c-axis.

Third, we discuss the influence of magnetic transition on electronic transport properties. Figure 3(a) presents the temperature dependence of longitudinal resistivity, $\rho_{xx}(T)$, measured at zero field. With decreasing temperature, the resistiv-

ity decreases at first, reaches a minimum at about 60 K, then increases before dropping again below T_N. The resistivity exhibiting a maximum at T_N is usually due to the scattering of local spins to the conduction electrons, which is also confirmed by the resistivity data measured at magnetic fields. As shown in the inset of Fig. 3(a), with increasing magnetic field, the resistivity around T_N is suppressed, and its maximum at T_N almost disappears. Figure 3(b) shows the magnetoresistance (MR) as a function of magnetic field measured at various temperatures, here MR is defined as

$$\mathrm{MR} = \frac{\rho(H)-\rho(0)}{\rho(0)} \times 100\%, \tag{2}$$

where $\rho(H)$ and $\rho(0)$ are the resistivities measured at a magnetic field H applied along the c-axis and zero-field, respectively. Below 50 K, the resistivity decreases with increasing magnetic field H, i.e., exhibiting a negative magnetoresistance behavior, and MR reaches -5%, at $\mu_0 H = 8$ T, $T = 1.8$ K, which can be ascribed to reducing spin scattering by the applied magnetic field.

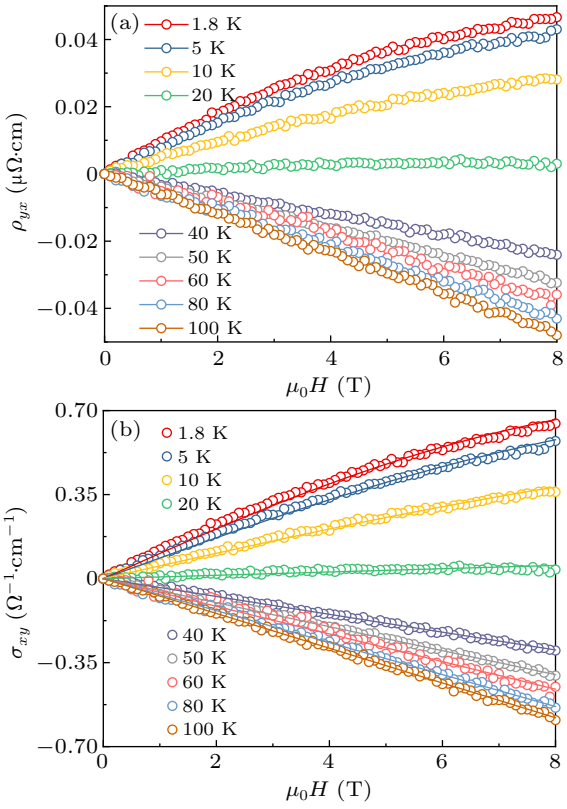


Fig. 4. (a) Field dependence of Hall resistivity, ρ_{yx}, measured at various temperatures for a $V_{1/3}TaS_2$ crystal. (b) Components of the conductivity tensor, i.e., σ_{xy} as a function of magnetic field for different temperatures (< 100 K). Hollow dots represent the experimental data and the solid lines are the fitting curves using the two-carrier model.

Finally, as mentioned above, the band structure calculations demonstrate that $V_{1/3}TaS_2$ is a magnetic semimetal, which is also confirmed by the Hall resistivity measurements. Figure 4(a) shows the Hall resistivity as a function of the magnetic field applied along the c-axis, $\rho_{yx}(H,T)$, measured at various temperatures (1.8 K–100 K). Both the nonlinear field dependence of $\rho_{yx}(H,T)$ below 20 K and the change in the slope of $\rho_{yx}(H,T)$ from a positive value below 10 K to negative one above 40 K imply the existence of multi-band structure. To parameterize the Hall data, we analyze the longitudinal and Hall resistivity using a two-carrier model, as we discuss for other semimetals.[24–29] In this model, the conductivity tensor in its complex representation is given as[30]

$$\sigma = e\left(\frac{n_e\mu_e}{1+\mathrm{i}\mu_e\mu_0 H} + \frac{n_h\mu_h}{1+\mathrm{i}\mu_h\mu_0 H}\right), \tag{3}$$

where n_e (n_h) and μ_e (μ_h) denote the carrier concentrations and mobilities of electrons (holes), e is the elementary charge, respectively. To appropriately evaluate the carrier densities and mobilities, we calculate the Hall conductivity $\sigma_{xy} = \rho_{yx}/(\rho_{xx}^2+\rho_{yx}^2)$ using the original experimental $\rho_{yx}(H,T)$ data. Then, as shown in Fig. 4(b), we fit $\sigma_{xy}(H,T)$ data using the fitting parameters and the field dependence given by[31]

$$\sigma_{xy} = e\left[\frac{(\mu_0 H)\, n_h\mu_h^2}{1+\mu_h^2(\mu_0 H)^2} - \frac{(\mu_0 H)\, n_e\mu_e^2}{1+\mu_e^2(\mu_0 H)^2}\right]. \tag{4}$$

The obtained n_e (n_h) and μ_e (μ_h) as a function of temperature are plotted in Fig. 5 and the inset. It is clear that both the n_e and n_h are almost independent of temperature below 20 K, such as $n_e(1.8\ \mathrm{K}) = 0.22\times10^{19}$ cm^{-3}, $n_e(20\ \mathrm{K}) = 0.34\times10^{19}$ cm^{-3}, $n_h(1.8\ \mathrm{K}) = 0.21\times10^{19}$ cm^{-3}, $n_h(20\ \mathrm{K}) = 0.54\times10^{19}$ cm^{-3}, and enhance markedly with increasing temperature, such as $n_e(100\ \mathrm{K}) = 8.2\times10^{19}$ cm^{-3}, $n_h(100\ \mathrm{K}) = 3.6\times10^{19}$ cm^{-3}. On the contrary, the mobility of the hole, μ_h, increases rapidly with decreasing temperature and is much larger than the μ_e at lower temperatures, although they are almost the same at higher temperatures. These behaviors are similar to those occurring in many other semimetals.[27,32]

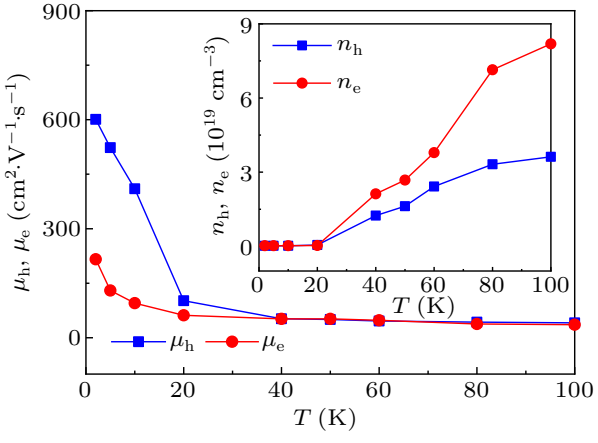


Fig. 5. The carrier mobilities, μ_h and μ_e, and (inset) the carrier concentrations n_h and n_e, as a function of temperature, extracted from the two-carrier model analysis of σ_{xy} data.

4. Conclusion

We performed electronic structure calculations and measured the longitudinal resistivity, Hall resistivity, and susceptibility on $V_{1/3}TaS_2$ crystals with a hexagonal noncentrosymmetric structure (space group $P6_322$). It was found that $V_{1/3}TaS_2$ is an A-type antiferromagnet with $T_N = 6.20$ K, and exhibits a negative MR near T_N. Both band structure calculation and Hall resistivity measurement demonstrated it is a magnetic semimetal.

Acknowledgments

Project supported by the National Key Research and Development Program of China (Grant No. 2022YFA1403202), the National Natural Science Foundation of China (Grant Nos. NSFC-12074335, 11974095, 5177115, 11974095, and 12188101), and the Natural Science Foundation of Shaanxi Province of China (Grant No. 2022JM-028).

References

[1] Gong C, Li L, Li Z, *et al.* 2017 *Nature* **546** 265
[2] Huang B, Clark G, Navarro-Moratalla E, *et al.* 2017 *Nature* **546** 270
[3] Deng Y, Yu Y, Song Y, *et al.* 2018 *Nature* **563** 94
[4] Chen B, Yang J, Wang H, Imai M, Ohta H, Michioka C, Yoshimura K and Fang M 2013 *J. Phys. Soc. Jpn.* **82** 124711
[5] Togawa Y, Kousaka Y, Nishihara S, Inoue K, Akimitsu J, Ovchinnikov A and Kishine J I 2013 *Phys. Rev. Lett.* **111** 197204
[6] Masaki Y, Aoki R, Togawa Y and Kato Y 2018 *Phys. Rev. B* **98** 100402
[7] Morosan E, Zandbergen H, Li L, Lee M, Checkelsky J, Heinrich M, Siegrist T, Ong N P and Cava R 2007 *Phys. Rev. B* **75** 104401
[8] Manzeli S, Ovchinnikov D, Pasquier D, Yazyev O V and Kis A 2017 *Nat. Rev. Mater.* **2** 17033
[9] Voiry D, Mohite A and Chhowalla M 2015 *Chem. Soc. Rev.* **44** 2702
[10] Zhao B, Shen D, Zhang Z, Lu P, Hossain M, Li J, Li B and Duan X 2021 *Adv. Funct. Mater.* **31** 2105132
[11] Morosan E, Zandbergen H W, Dennis B S, Bos J W, Onose Y, Klimczuk T, Ramirez A P, Ong N P and Cava R J 2006 *Nat. Phys.* **2** 544
[12] Rahman A, Rehman M U, Kiani M, Zhao H, Wang J, Lu Y, Ruan K, Dai R, Wang Z, Zhang L, Wang J and Zhang Z 2022 *Phys. Rev. B* **105** 144413
[13] Kousaka Y, Ogura T, Zhang J, Miao P, Lee S, Torii S, Kamiyama T, Campo J, Inoue K and Akimitsu J 2016 *J. Phys.: Conf. Ser.* **746** 012061
[14] van den Berg J M and Cossee P 1968 *Inorganica Chim. Acta* **2** 143
[15] Nakanishi M, Matsuno Y, Fujii T, Takada J and Yoshimura K 2008 *J. Phys. Chem. Solids* **69** 49
[16] Ghimire N J, Botana A S, Jiang J S, Zhang J, Chen Y S and Mitchell J F 2018 *Nat. Commun.* **9** 3280
[17] Lu K, Sapkota D, Debeer-Schmitt L, Wu Y, Cao H B, Mannella N, Mandrus D, Aczel A A and MacDougall G J 2020 *Phys. Rev. Mater.* **4** 054416
[18] Kresse G and Furthmüller J 1996 *Comput. Mater. Sci.* **6** 15
[19] Kresse G and Furthmüller J 1996 *Phys. Rev. B* **54** 11169
[20] Perdew J P, Burke K and Ernzerhof M 1996 *Phys. Rev. Lett.* **77** 3865
[21] Kresse G and Joubert D 1999 *Phys. Rev. B* **59** 1758
[22] Parkin S S and Friend R H 1980 *Physica B+C* **99** 219
[23] Karna S K, Womack F, Chapai R, *et al.* 2019 *Phys. Rev. B* **100** 184413
[24] Zhou Y, Lou Z, Zhang S, *et al.* 2020 *Phys. Rev. B* **102** 115145
[25] Chen S, Lou Z, Zhou Y, Chen Q, Xu B, Wu C, Du J, Yang J, Wang H and Fang M 2021 *Chin. Phys. Lett.* **38** 017202
[26] Chen Q, Zhou Y, Xu B, *et al.* 2021 *Chin. Phys. Lett.* **38** 087501
[27] Chen Q, Lou Z, Zhang S, *et al.* 2020 *Phys. Rev. B* **102** 165133
[28] Du J, Wang H, Chen Q, *et al.* 2016 *Sci. China Phys. Mech.* **59** 657406
[29] Du J, Lou Z, Zhang S, *et al.* 2018 *Phys. Rev. B* **97** 245101
[30] Ali M N, Xiong J, Flynn S, *et al.* 2014 *Nature* **514** 205
[31] Zhou Q, Rhodes D, Zhang Q, Tang S, Schönemann R and Balicas L 2016 *Phys. Rev. B* **94** 121101
[32] Hu J, Tang Z, Liu J, *et al.* 2016 *Phys. Rev. Lett.* **117** 016602